Measurement of the Thermal Conductivity of Carbon Nanotube–Tissue Phantom Composites with the Hot Wire Probe Method

ARTICLE *in* ANNALS OF BIOMEDICAL ENGINEERING · MARCH 2011

Impact Factor: 3.23 · DOI: 10.1007/s10439-011-0268-7 · Source: PubMed

Annals of Biomedical Engineering, Vol. 39, No. 6, June 2011 *(© 2011)* pp. 1745–1758
DOI: 10.1007/s10439-011-0268-7

Measurement of the Thermal Conductivity of Carbon Nanotube–Tissue Phantom Composites with the Hot Wire Probe Method

SAUGATA SARKAR,[1] KRISTEN ZIMMERMANN,[2] WEINAN LENG,[3] PETER VIKESLAND,[3] JIANFEI ZHANG,[4] HARRY DORN,[4] THOMAS DILLER,[1] CHRISTOPHER RYLANDER,[1,2] and MARISSA NICHOLE RYLANDER[1,2]

[1]Department of Mechanical Engineering, Virginia Polytechnic Institute and State University, ICTAS Building, Stanger Street, MC0298, Blacksburg, VA 24061, USA; [2]School of Biomedical Engineering and Sciences, Virginia Tech-Wake Forrest University, ICTAS Building, Stanger Street, MC0298, Blacksburg, VA 24061, USA; [3]Department of Civil and Environmental Engineering, Virginia Polytechnic Institute and State University, 415 Durham Hall, Blacksburg, VA 24061, USA; and [4]Department of Chemistry, Virginia Polytechnic Institute and State University, 1109 Hahn Hall South, Blacksburg, VA 24061, USA

(Received 18 May 2010; accepted 3 February 2011; published online 1 March 2011)

Associate Editor James Tunnell oversaw the review of this article.

Abstract—Developing combinatorial treatments involving laser irradiation and nanoparticles require an understanding of the effect of nanoparticle inclusion on tissue thermal properties, such as thermal conductivity. This information will permit a more accurate prediction of temperature distribution and tumor response following therapy, as well as provide additional information to aid in the selection of the appropriate type and concentration of nanoparticles. This study measured the thermal conductivity of tissue representative phantoms containing varying types and concentrations of carbon nanotubes (CNTs). Multi-walled carbon nanotubes (MWNTs, length of 900–1200 nm and diameter of 40–60 nm), single-walled carbon nanotubes (SWNTs, length of 900–1200 nm and diameter <2 nm), and a novel embodiment of SWNTs referred to as single-walled carbon nanohorns (SWNHs, length of 25–50 nm and diameter of 3–5 nm) of varying concentrations (0.1, 0.5, and 1.0 mg/mL) were uniformly dispersed in sodium alginate tissue representative phantoms. The thermal conductivity of phantoms containing CNTs was measured using a hot wire probe method. Increasing CNT concentration from 0 to 1.0 mg/mL caused the thermal conductivity of phantoms containing SWNTs, SWNHs, and MWNTs to increase by 24, 30, and 66%, respectively. For identical CNT concentrations, phantoms containing MWNTs possessed the highest thermal conductivity.

Keywords—Thermal properties, Sodium alginate, Carbon nanoparticle, Thermal conductance, Hyperthermia, Laser therapy.

Address correspondence to Marissa Nichole Rylander, School of Biomedical Engineering and Sciences, Virginia Tech-Wake Forrest University, ICTAS Building, Stanger Street, MC0298, Blacksburg, VA 24061, USA. Electronic mail: saugata@vt.edu, mnr@vt.edu

INTRODUCTION

Laser therapies can provide a minimally invasive alternative to surgical resection of malignant tumors; however, their effectiveness is limited by nonspecific heating of target tissue, which can lead to healthy tissue injury. Inclusion of optically absorbing and thermally conductive nanoparticles, such as carbon nanotubes (CNTs), in laser therapy has the potential to increase heat generation and tumor destruction. Furthermore, integration of highly thermally conductive CNTs can enhance the overall thermal conductivity of the tissue, thereby increasing thermal diffusion within the tissue and allowing treatment of larger tumor volumes.

CNTs have received significant attention for their potential role as thermal enhancers for laser ablation and drug delivery.[3,30] CNTs are composed of graphene sheets with sp^2 bonded carbon atoms rolled seamlessly into a tubular form. The two major types of CNTs are single-walled carbon nanotubes (SWNTs), which are seamless individual tubes, and multi-walled carbon nanotubes (MWNTs), which possess two or more concentric tubes. The diameter and length of SWNTs are 1.5–3.0 nm and 20–1000 nm, respectively, whereas the corresponding dimensions are 5.0–100 nm and 1–50 μm for MWNTs.[14,35,37,44] Another more unique embodiment of SWNTs are single-walled carbon nanohorns (SWNHs), which are hollow, conical tubules of single sheet graphene with agglomerate diameters of 50–100 nm.[17,29] Throughout this paper, we refer to SWNTs, MWNTs, and SWNHs as CNTs for brevity. All of the previously mentioned CNT

structures possess significant ability to absorb electromagnetic signals in the near infrared region (NIR) (700–1100 nm) leading to considerable heat generation that permits tumor cell destruction.[9,19,35,36,45,48,49,54,60] NIR light is transmitted through tissue such as skin with scattering-limited attenuation and minimal heating. Light within this optical window can penetrate tissue at depths beyond 1.6–2.0 mm with irradiances well below the threshold for normal tissue damage.[1] Previous studies have shown that excitation of CNTs with a laser wavelength of 1064 nm (known to possess clinical relevance due to an estimated light penetration depth of several millimeters) can cause significant light absorption, heat generation, and tumor cell death.[9,19,45,49,54] Other groups have successfully measured the absorbance of various nanoparticles used for similar applications (C_{60}, gold nanoshells, gold nanorods, etc.).[23,25,32] However, CNTs have been shown by our group and others to possess greater capability for optical absorption compared to fullerenes (e.g., C_{60}) and gold nanoshells/nanorods due to their exceptional antenna properties.[9,32,45,49]

CNTs have extraordinary electromagnetic, thermal, optical, and chemical properties. They exhibit very high thermal conductivity (3000–6000 W/m·K)[7,16,20,27,57] compared to the thermal conductivity of tissue and tumors, which vary from 0.511 to 0.561 W/m·K.[26,51] Therefore, inclusion of CNTs into the tissue has the potential to enhance the overall thermal conductivity of the tissue. Varying the CNT type and concentration is hypothesized to have a significant impact on tissue thermal conductivity and heat diffusion within the tissue. However, the impact of CNT inclusion on the tissue thermal conductivity is unknown and is critical to determining the associated heat diffusion in a three-dimensional tissue following laser excitation. A more comprehensive understanding of the impact of CNT inclusion on the overall tissue thermal conductivity would enable better prediction of the size of the treatment volume following therapy. Ultimately, this knowledge would allow optimization of laser parameters (e.g., laser irradiance and duration) and CNT properties (e.g., length, concentration) to achieve better correspondence between the treated region and desired therapy margins. Treatment planning models can be utilized for designing CNT-enhanced laser therapies, but effective prediction and optimization of tissue response require knowledge of the appropriate input thermal properties, such as thermal conductivity.

The effect of thermal conductivity at the CNT–liquid interface has been characterized by measuring the interfacial thermal conductance between CNTs and liquid solvents.[28,34] Interfacial thermal conductance is defined as $q'' = -U \cdot \Delta T = -\Delta T/R''$, where q'' is the heat flux, ΔT is the temperature difference, U is the interfacial thermal conductance, and R'' is the interfacial thermal resistance between the nanoparticle and its surroundings. Huxtable *et al.*[28] used picosecond transient absorption to measure the interfacial thermal conductance (inverse of resistance) of CNTs suspended in surfactant micelles in water. They determined the CNT composite thermal conductivity was limited by exceptionally small interfacial thermal conductance ($G = 12$ MW/m^2/K). Merabia *et al.*[34] described the interfacial thermal conductance of gold nanoparticles in octane and in water by molecular dynamics (MD). For this case, interfacial thermal conductance was determined to be 50–100 MW/m^2/K in octane and 150–170 MW/m^2/K in water for laser powers of 150–700 nW. Small interfacial thermal conductance corresponds to high interfacial thermal resistance, which impacts the overall thermal conductivity of the CNT composite. Therefore, a hypothesis can be made that large interfacial thermal resistance will reduce the overall thermal conductivity of the CNT–tissue composite compared to the intrinsic thermal conductivity of the CNT. Nan *et al.*, Bryning *et al.*, Clancy *et al.*, and Gao *et al.* also determined the overall thermal conductivity of CNT composites with and without interfacial thermal resistance computationally by using an effective medium approach (EMA).[8,12,21,40,41] This study concluded that the presence of interfacial thermal resistance reduced the overall thermal conductivity of CNT composites significantly. However, when the CNT formed a perfect interface with the polymer matrix, interfacial thermal resistance was negligible and the thermal conductivity of the CNT composite was increased 5–20 times (depending on diameter and aspect ratio) compared to the thermal conductivity in the presence of interfacial thermal resistance.[41]

The thermal conductivity of human and animal tissues has been found to vary from 0.5–0.58 W/m·K in previous literature.[4,13,15,33,43] Tissue representative phantoms made of agar or sodium alginate have been used for representative tissue systems due to their similar thermal and optical properties to tissue.[31,45,55] Thermal conductivity of agar gel phantoms (95% water content) has been measured and the values have been determined to be in the range of 0.576–0.585 W/m·K.[58] Due to a similar water content, thermal conductivity of sodium alginate phantoms (97% water), agar phantoms (95%), and animal or human tissues (>85% water) can be assumed to be nearly identical. No prior studies have measured the overall thermal conductivity of tissues with inclusion of CNTs; therefore, little is known regarding the true impact of CNT inclusion on the overall heat diffusion properties of a tissue matrix.

There are several methods for measuring the thermal conductivity of soft tissue and each method possesses inherent advantages and challenges. It is difficult

to measure the thermal conductivity of a soft tissue due to the challenges in designing an apparatus for steady state or quasi-steady state measurements. Traditionally, thermal conductivities of soft tissues have been measured by guarded-hot plates.[24,43] In this method, a tissue sample is placed between two electrical heater plates at different temperatures. Heat is allowed to flow from the hotter plate to the colder plate until steady state conditions are reached, at which time temperature is measured. However, this method has difficulty in bringing the samples to steady state conditions and requires significant periods of time, which leads to dehydration of the sample and corresponding changes in thermal properties. This method also requires complex solution methods involving two- or three-dimensional heat transfer analysis. Other techniques have been developed to measure thermal conductivity of biological samples more rapidly using transient heat transfer methods. Among them is the dual-thermistor probe method,[59] which uses two thermistor beads, consisting of a heater and sensor, which are placed in a sample at specific distances so that thermal diffusion can be measured accurately by the sensor. The dual-thermistor probe method is highly invasive and is not suitable for *in vivo* experiments; however, this method is amenable for measurement of liquid samples, such as blood plasma, skimmed milk, etc. Another thermal conductivity measurement alternative is the pulse-decay method,[2] which utilizes a microprobe resistor to provide several square-wave heating pulses. The temperature decay is then measured with a sensor attached to the microprobe resistor. This method is suitable for liquid samples and has been utilized to determine the thermal conductivity of silicon oil and glycerin;[2,59] however, it is complex and involves an elaborate microprobe fabrication process.

A more simple and accurate technique called the hot wire probe method[4,5,22,33] has recently been used to measure thermal conductivity of *in vivo* and *ex vivo* samples. This method is minimally invasive and utilizes transient heat diffusion analysis to compute the thermal conductivity. A single line heat source, called a hot wire probe, acts as a heater and temperature sensor, allowing measurement of the time dependent temperature response from the surface of the probe. This method requires minimal time and experimental setup to measure temperature response and thermal conductivity. Therefore, minimal water content is removed from samples and thermal properties remain unchanged during the experiment. For this method, the samples are built with a high aspect ratio (the sample is considered infinitely long) so that any axial heat flow is negligible. Therefore, only 1-dimensional (1-D) radial heat transfer is considered in the analysis. This method has been utilized by numerous groups to measure the thermal conductivity of glycerine[33] (a.k.a glycerol), hard black rubber,[33] foamed plastics,[33] agar gel,[58] and Styrofoam.[4] The accuracy for measuring the thermal conductivity of liquid and solid samples using the hot wire probe method has been confirmed through comparison with thermal conductivity determined by the steady state thin film approach,[46] dual-thermistor probe method,[59] pulse-decay method,[11] and the guarded-hot plate method.[24,43]

In this paper, a hot wire probe was created and utilized to measure thermal conductivity of tissue representative, sodium alginate phantoms containing varying CNT types (SWNTs, MWNTs, and SWNHs) and concentrations (0.1, 0.5, and 1.0 mg/mL). Concentrations of CNTs lower than 1.0 mg/mL were utilized because this threshold concentration has been shown to cause minimal toxicity.[9,48,49] This CNT concentration when combined with laser heating has produced significant heat generation, thermal based tumor destruction, and tumor regression in both *in vitro* and *in vivo* studies.[9,39,45,49,52] Knowledge of the impact of CNT type and concentration on thermal conductivity will permit more accurate prediction of temperature distribution and tumor response following therapy, as well as guide selection of the type and concentration of nanoparticles to maximize thermal diffusion in the targeted zone. This knowledge will also aid in development of computational treatment planning models for laser therapies utilizing CNTs by providing more accurate thermal conductivity input properties necessary for temperature prediction within the treated tissue.

MATERIALS AND METHODS

Hot Wire Probe

The hot wire probe was constructed from high precision stainless steel tubes, nichrome wire, and thermocouples. Two stainless steel tubes with outer diameters (ODs) of 0.635 mm (inner tube) and 1.47 mm (outer tube, d) were cut into 50 mm long (L) pieces (Fig. 1a) to provide an aspect ratio (L/d) of 34. Blackwell *et al.*[6] determined that the aspect ratio must be greater than 25 in order to minimize axial heat transfer in the probe. The inner tube was coiled tightly with a nichrome wire (a heater coil with diameter 0.0031 inch, Pelican Wire Company, FL). The coiling process was done with care, to prevent an air gap or overlap between the coils (Fig. 1b). The presence of an air gap could increase local thermal resistance and likelihood of burn out of the heater during the experiment. The inner tube with the nichrome coil was then dipped into highly conductive Ceramabond aluminum nitride solution (Armeco Products Inc., NY) to create

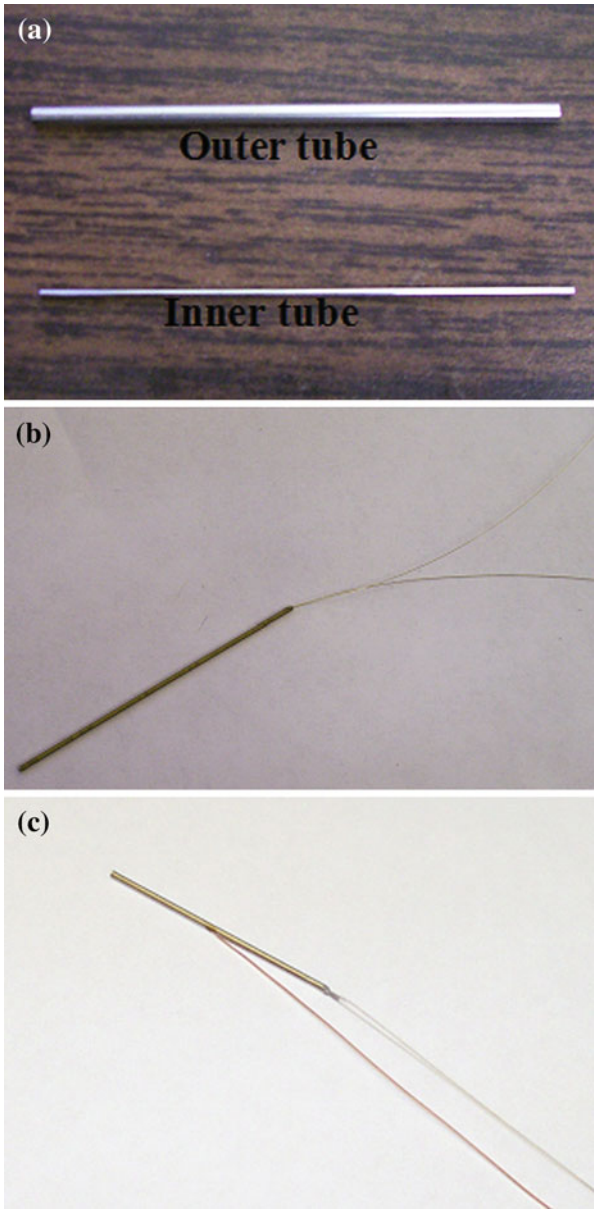

FIGURE 1. Development of hot wire probe. Two high precision stainless steel tubes, inner tube (OD: 0.635 mm), and outer tube (OD: 1.47 mm), were cut into 50 mm pieces (a). The inner tube was coiled with nichrome wire (b). The hot wire probe (c) was completed by placing the coiled inner tube (b) into the outer tube. A K-type thermocouple was welded to the middle of the surface of the outer tube (c).

a coating around the coil and placed into the outer tube (Fig. 1c) to eliminate an air gap between the coil and the outer tube. A thermocouple (K-type) was welded to the middle of the outer tube in order to measure temperature response (Fig. 1c).[4,33]

Measurement Theory

Thermal conductivities of tissue phantoms alone or with CNTs of varying type (MWNT, SWNT, and SWNH) and concentrations (referred to as CNT–phantom composites) were measured using the cylindrical hot wire technique.[4,5,22,33] The governing equation used for this method is described below.

$$\frac{\partial^2 T}{\partial r^2} + \frac{1}{r}\frac{\partial T}{\partial r} = \frac{1}{\alpha}\frac{\partial T}{\partial t} \tag{1}$$

Equation (1) is a 1-D transient heat transfer equation in cylindrical coordinates, where T is the temperature, r is the position, t is the time, and α is the thermal diffusivity. The solution[10] of Eq. (1) is expressed as:

$$T - T_{\mathrm{i}} = -(q'/4\pi K)E_{\mathrm{i}}(-r^2/4\alpha t) \tag{2}$$

where T_{i} is the uniform initial temperature at time $t < 0$, K (W/m·K) is the thermal conductivity, and q' (W/m) is the constant heat source applied to the heater probe at $t > 0$ and is represented by $q' = \frac{V^2}{R \cdot L}$, where V is the voltage, R is the resistance, and L is the length of the heat source. $E_{\mathrm{i}}(-x)$ is the exponential integral function which is defined as:

$$E_{\mathrm{i}}(-x) = -\gamma + \ln x + \sum_{n=0}^{\infty} \frac{(-x)^n}{n \times n!}; \quad \text{when } x > 0 \tag{3}$$

where $\gamma = 0.5772$ is Euler's constant.

Equation (3) can be reduced to the first two terms for the condition of $r^2/4\alpha t < (0.16)^2$ by eliminating the infinite summation component[42] and expressed as Eq. (4).

$$T - T_{\mathrm{i}} = \frac{q'}{4\pi K}\left[\ln\left(\frac{4\alpha t}{r^2}\right) - \gamma\right] \tag{4}$$

After differentiating Eq. (4) and solving for K, the following equation is obtained.

$$K = \frac{q'}{4\pi}\left(\frac{dT}{d\ln(t)}\right)^{-1} \tag{5}$$

If the slope, $\frac{dT}{d\ln(t)}$, is known, K can be measured from Eq. (5).

In order to avoid the outer surface effects of the sample on the temperature rise of the heater probe, the following criterion must be satisfied for a 1-D model:

$$R_0 > 2(\alpha t)^{1/2} \tag{6}$$

where R_0 is the outer radius of the sample. When this criterion is satisfied, the effect of surface conditions on the temperature response is less than 0.1%, and a linear relationship is formed between the temperature response and logarithmic time.[4,33] If the heating time is less than 5 min and the thermal diffusivity, α, is 1.4×10^{-7} m^2/s (e.g., water, pig tissue, or any sample more than 90% of water), the minimum outer radius of

a sample, R_0, can be calculated to be 12.9 mm from Eq. (6). For these samples with thermal diffusivities close to water, a linear temperature response is found for a heating time of approximately 5 min. For longer durations, the linear temperature response becomes nonlinear and surface conditions begin to affect the probe temperature. The linearity of temperature response is critical since the thermal conductivity will be determined from the slope of the temperature response in the linear region.

Sample Preparation

Agar Gel Phantoms

Agar gel, glycerol, and Styrofoam, with previously measured thermal conductivities, were all used for calibration and confirmation of the accuracy of the hot wire probe. Agar gel phantoms (used for initial validation of hot wire probe accuracy) were made by dissolving 5 g agar in 100 mL water. Agar was uniformly mixed in boiling water and cooled rapidly in ice water. After 12 h at 4 °C, the sample became solidified to allow measurement. Six samples each of Agar gel, glycerol, and Styrofoam were created and used for thermal conductivity measurement.

CNT Phantoms

SWNTs were purchased from SES Research, Inc. (Houston, TX), MWNTs (Nano lab, Inc., MA) were provided by Dr. David Carroll's research group at Wake Forest University (20 h sonication in 70% sulfuric acid and 30% nitric acid of the total volume), and SWNHs were provided by Dr. David Geohegan's laboratory at Oak Ridge National Laboratories (Oak Ridge, TN). The purity of all CNTs was confirmed to be greater than 95% by thermogravimetric analysis (TGA) and transmission electron microscopy (TEM) (data not shown). The length of the MWNTs and SWNTs was 900–1200 nm. The outer diameters of the MWNTs were 40–60 nm, whereas the outer diameters of the SWNTs were less than 2 nm. Individual SWNHs had diameters of 3–5 nm and lengths of 25–50 nm and formed aggregates with overall diameters of 50–100 nm.

MWNTs, SWNTs, and SWNHs are naturally hydrophobic and are minimally soluble in polar solvents such as water. The solubility of each CNT type was enhanced by non-covalently functionalizing their outer surfaces with 1% w/v Pluronic F-127 purchased from Biotium, Inc. (Hayward, CA). This process forms a hydrophilic layer around the CNTs without changing their thermal, optical, or mechanical properties.[9,49] Previous studies have shown this amount of Pluronic is sufficient to disperse CNTs in aqueous solutions, while maintaining minimal toxicity during *in vitro* and *in vivo* studies.[9,49] CNTs in the Pluronic water suspensions were sonicated for 30–40 min to create three suspensions with desired concentrations (0.1, 0.5, and 1.0 mg/mL).

Tissue representative phantoms were prepared from sodium alginate Protanal LF 10/60 (FMC Biopolymer, Drammen, Norway), a low viscosity alginate with a mean guluronate/mannuronate (G/M) ratio of 70% and mean molecular weight of 180 kDa. Sodium alginate powder was mixed with the CNT–Pluronic water suspensions described above to a 3% w/v concentration (3 g/100 mL) for 1 h to create the desired final concentrations of CNTs in alginate solution. CNT dispersions in liquid alginate at 4 °C were monitored before and after cross-linking for 1 month. No precipitation of CNTs in 3% sodium alginate suspensions was observed after several weeks of storage at 4 °C, as evidenced by a homogeneous dark phantom. Prior to the measurement of thermal conductivity, the sodium alginate–CNT mixture was cross-linked with 80 mM calcium chloride (Sigma-Aldrich, St. Louis, MO) for several weeks[31,55] to completely solidify the sample. The sodium alginate phantoms had a radius of 15.75 mm and a length of 120 mm. These dimensions permitted the samples to be amenable to 1-D radial heat diffusion analysis[6] with minimal influence of surface conditions. Ten types of tissue representative phantoms were prepared with six samples ($n = 6$) for each type. Nine types of phantoms were prepared with inclusion of MWNTs, SWNTs, and SWNHs at three different concentrations (0.1, 0.5, and 1 mg/mL) and one phantom without CNTs to serve as a control.

Characterization of CNT Stability in Suspension

After functionalizing CNTs with 1% Pluronic, the quality and extent of CNT dispersions in the aqueous solutions were monitored for several months. No precipitation of CNTs was observed and the suspension coloration remained homogenous. To further confirm the stability of CNTs in aqueous solution, dynamic light scattering (DLS) and electrophoretic light scattering (ELS) were conducted. DLS measurements were performed with an ALV/CGS-3 compact goniometer system and ALV/LSE-5003 multi-τ digital correlator at 25 °C. A He–Ne laser producing vertically polarized light of $\lambda_0 = 632.8$ nm was used as a light source. SWNHs, SWNTs, and SWNHs were sonicated in a 1% (w/v) Pluronic solution for 40 min to obtain 0.05 mg/mL CNT suspensions. DLS was conducted 1 week after the suspensions were produced.

ELS was conducted to obtain a zeta potential value for each sample using a Malvern Zetasizer Nano-ZS

system (Worcestershire, UK). CNTs in 1% (w/v) Pluronic solutions were placed into a folded capillary cell (Malvern Instruments, Worcestershire, UK) and were irradiated with a 632.8 nm He–Ne laser.

Characterization of CNT Stability in Phantoms

To verify the homogeneity of CNT dispersion in cross-linked samples, phantoms were sectioned into 50–60 nm thick sections by a microtome at the top, middle, and bottom positions within the phantom. High resolution transmission electron microscopy (Zeiss 10CA TEM, Carl Zeiss SMT Inc., Peabody, MA) was performed on five samples from each location.

Raman spectroscopy was also used to characterize the homogeneity of CNT–phantom composites as a supplement to TEM imaging. A Witec Alpha500R system (Ulm, Germany) was used and spectra were obtained using 785 nm laser excitation, 300 line/mm diffraction grating, and a 10× objective (Olympus, N.A. = 0.3). The laser power used for all measurements was less than 5 mW for each sample. Small discs of CNT–sodium alginate phantoms were made for Raman mapping to acquire a flat surface. Briefly, SWNTs, MWNTs, and SWNHs in sodium alginate were prepared as described above. Concentrations of 1.0 mg/mL were used for Raman spectroscopy to enhance the carbon nanoparticle signal. CNT–sodium alginate mixtures were then poured into a washer (inner diameter: 3.8 cm; thickness: 1.5 mm) and sandwiched between two membranes (5.0 μm pore size). Subsequently, the mixtures were cross-linked in an 80 mM $CaCl_2$ solution. All samples remained submerged in DI water throughout the measurements. Four 25 × 25 μm scans were performed per sample with a step size of 0.5 μm and an integration time of 0.1 s (MWNT and SWNH) or 0.02 s (SWNT) at each step. Longer integration times were used for MWNTs and SWNHs because their Raman signals were much weaker than that of the SWNTs. The Raman spectra for each step over the four scans were then averaged and the relative standard deviations of Raman intensities were calculated for the SWNT, MWNT, and SWNH–phantoms.

Experimental Setup

Agar gel, glycerol, Styrofoam, and all sodium alginate phantoms with and without CNTs were submerged in a water bath and maintained at a temperature of 24 °C to avoid any temperature fluctuation at the sample boundary. A heater probe with length of 50 mm pierced the middle of the sample and was connected to a power source as shown in Fig. 2. All materials were heated for 5–10 min depending on the maximum heating time calculated in Eq. (6) by applying a voltage of 5 V. The thermocouple of the heater was attached to a data acquisition system (National Instruments, NI 9211) and the time dependent temperature response was measured using the VI Logger from LabVIEW software. For initial calibration of the hot wire probe, thermal conductivities of agar gel, glycerol, and Styrofoam were measured ten times. Tissue phantoms with and without CNTs were each measured five times. Following each measurement, samples were allowed to equilibrate to the water bath temperature before repeating the measurement, and the probe was inserted into an identical position within each sample.

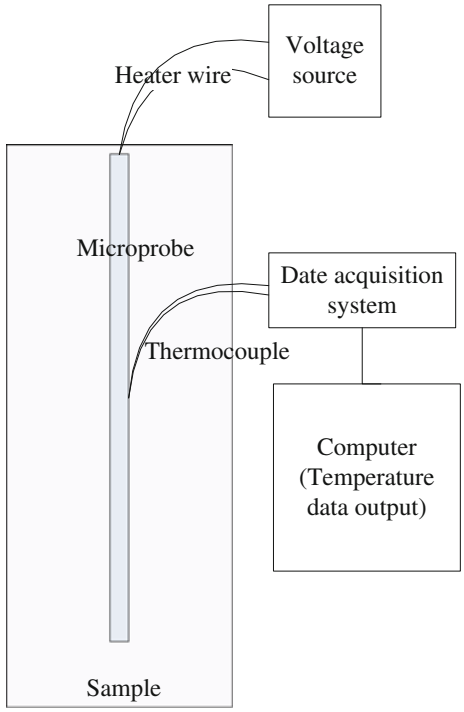

FIGURE 2. Schematic diagram of the experiment.

Uncertainty Analysis

Uncertainties and sensitivities[18,38] of all experimentally measured parameters were determined in order to calculate estimated errors in the thermal conductivity measurement. Thermal conductivities were represented in terms of experimentally measured parameters, i.e., slopes of the temperature responses (S) and prescribed values of heat sources (q') in Eq. (5). The total estimated uncertainty (δK) of the thermal conductivity measurements was computed by the method of propagation of uncertainties in Eq. (7)[38]

$$\delta K = \left\{ \sum_{i=1}^{N} \left(\frac{\partial K}{\partial X_i} \delta u_i \right)^2 \right\}^{1/2} \tag{7}$$

where $\frac{\partial K}{\partial X_i}$ is the sensitivity coefficient of thermal conductivity with respect to each of the parameters, X_i (slopes and heat sources), and δu_i is the uncertainty for a specific parameter X_i. We determined the standard deviation for each type of sample using established methods.[18]

The uncertainties and sensitivities[18,38] of all experimentally measured parameters associated with our hot wire probe system were determined in order to calculate estimated sources of error in the thermal conductivity measurements. The uncertainty of the temperature measurement (±0.05 °C) was associated with the data acquisition system, the thermocouples, and the electronic balance (concentration measurement error). Uncertainties of voltage (±0.025 V) and resistance (±2.16 Ω) measurements were associated with the power source and were utilized to determine the uncertainty of heat sources (q') by the method of propagation of uncertainties.[18] Uncertainty of temperature measurement was utilized to determine the uncertainty of slopes (S). Uncertainties of slopes (S) and heat sources (q'), and sensitivities of thermal conductivities with respect to slopes and heat source are presented in Table 1. These values were employed to compute the total estimated uncertainty of our hot wire probe for determining thermal conductivity, which was found to be 5.46%. The majority of estimated uncertainty arose from the slopes, which were used to determine thermal conductivity.

RESULTS

Validation of Heater Probe

To confirm the accuracy of our method, we measured the thermal conductivity of standard substances, such as agar gel (Acros Organics, Morris Plains, NJ) (0.05 g/mL in water), glycerol (Fisher Scientific, Inc., Pittsburgh, PA), and Styrofoam, with the hot wire probe method and compared our measurements with published data by other groups using the hot wire probe,[4] dual-thermistor,[59] pulse-decay,[11] and guarded-hot plate[24,43] techniques. Our measured data using the hot wire probe method[4,58] is similar to reported thermal conductivity values of Touloukian *et al.*[50] for glycerol, Styrofoam, and agar gel measured by steady state thin film approach[46] (Table 2). With our hot wire probe method, the corresponding standard deviations of agar gel, glycerol, and Styrofoam were determined to be ±0.012994, ±0.01562, and ±0.00024, respectively. The uncertainty analysis estimated errors (determined from total estimated uncertainty of 5.46% in Table 1) for agar gel, glycerol, and Styrofoam were calculated to be ±0.0155, ±0.0157, and ±0.00079, respectively. This indicates that the standard deviations are within the error limits of the uncertainty analysis.

TABLE 1. Estimated uncertainties and sensitivity coefficients of the experiment.

Parameters	Slope (S)	Heat source (q')	Total estimated uncertainty (%)
Δu_i	0.139 K/s	0.0241 W/m	5.46
$\partial K/\partial x_i$	4.526 W/m/s^2/K^2	0.4411 s/K	

Influence of Time on Heater Probe Measurement

The temperature response of all samples consisted of both linear and nonlinear components with respect to the natural logarithm of time. For agar gel samples, the linear response of temperature became nonlinear at approximately 7 min ($\ln(t) \sim 4$) due to the surface effects of the samples of 15.75 mm radius (Fig. 3). The calculated maximum heating time to maintain a linear temperature response was 7 min 23 s from Eq. (6) with $\alpha = 1.4 \times 10^{-7}$ m^2/s and sample radius of $R_0 = 15.75$ mm. Beyond this time, the temperature response became nonlinear and the surface temperature of samples is affected by the temperature rise of the heater probe. The close correspondence between the calculated time and the experimentally measured

TABLE 2. Comparison of measured values with previously reported values.[50]

	Thermal conductivity (W/m·K)	
Samples	Measured ± uncertainty	Previously reported
Agar gel (0.05 g/mL)	0.5662 ± 0.0155	0.567
Glycerol	0.2872 ± 0.0157	0.286
Styrofoam	0.0292 ± 0.00079	0.029

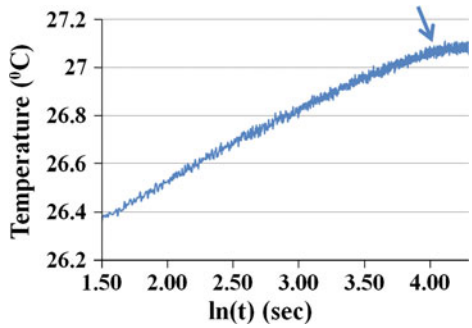

FIGURE 3. Temperature response of agar gel of radius 15.75 mm. Arrow indicates when linear response becomes non-linear at approximately 7 min ($\ln(t) \sim 4$) due to the influence of surface effects.

value (Fig. 3) further confirms the accuracy of the probe measurement.

Influence of Voltage

Prior to measurement of the thermal conductivity of all phantoms containing CNTs, different voltages (5 and 8 V) were applied to the agar gel to determine the effect of voltage on thermal conductivity. Thermal conductivity was measured for six different agar gel samples and each sample was measured ten times. For each voltage, the average temperature response was represented with logarithmic time (Figs. 4a, 4b). The slope of each temperature response was measured from regression of the linear portion (from $\ln(t) = 1.35$–3 s). In this region, the curve fit yielded R^2 values of 0.9785 and 0.9913 for 5 V and 8 V, respectively, indicating accuracy of the linear regression. The lower voltage of 5 V contributes to higher noise for the temperature response and results in a lower R^2 value compared to the higher voltage (8 V). The slope $(dT/d\ln t)$, determined by linear regression from Figs. 4a and 4b, was used in Eq. (5) and thermal conductivities for the agar gel samples were calculated to be 0.568 and 0.5889 W/m·K for 5 and 8 V, respectively, with corresponding standard deviations of ±0.012994 and ±0.011, respectively. Due to the similarity of the thermal conductivity values, it is evident that varying the voltage had minimal effect on thermal conductivity measurement.

Thermal Conductivity of Phantoms Without CNTs

We utilized 5 V when performing all subsequent measurements of thermal conductivity for sodium alginate phantoms with and without CNT inclusion with a sample size of six for each control group in order to avoid thermal damage to the heater probes. Figure 5 represents the average temperature response with respect to logarithmic time for sodium alginate phantoms (3 g in 100 mL water) without CNT inclusion. The slope of the temperature response is 0.1809 K/s with an R^2 value of 0.9792, determined by linear regression in the range of $\ln(t)$ values from 1.35 to 3 s. The thermal conductivity of the control phantom was calculated to be 0.5737 W/m·K with standard deviation of ±0.0146 using Eq. (5). From uncertainty analysis, the error was calculated to be ±0.0157 for sodium alginate phantoms. The standard deviation was again confirmed to be within the range of uncertainty. Therefore, uncertainty analysis was used subsequently to determine errors for other phantoms containing CNTs. The thermal conductivity of sodium alginate phantoms was determined to be similar to the agar gel, which is likely due to the comparable volume of water content. The high water content (>95%) of sodium alginate phantoms caused their thermal conductivity to be nearly identical to mineral water (0.6 W/m·K).[50]

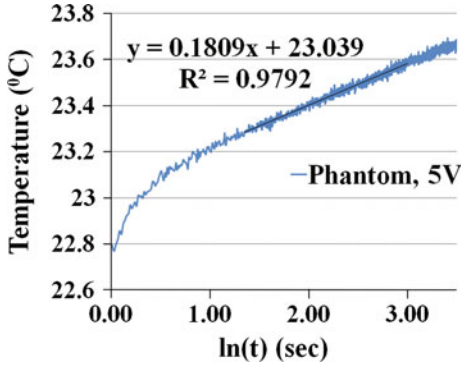

FIGURE 5. Temperature response of sodium alginate phantom without CNTs using 5 V supply. The slope of the linear portion is 0.1809 K/s and the thermal conductivity was calculated to be 0.5737 W/m·K.

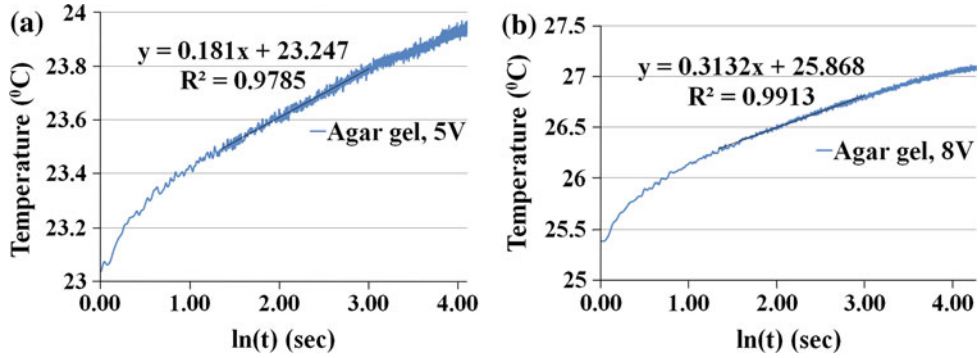

FIGURE 4. Temperature response of agar gel vs. the natural log of time due to various voltages. (a) 5 V supply yielded a slope of the linear portion of 0.181 K/s and corresponding thermal conductivity of 0.568 W/m·K and (b) 8 V supply yielded a slope of the linear portion of 0.3132 K/s and thermal conductivity of 0.5889 W/m·K.

Characterization of CNT Stability

Since the extent of CNT dispersion will affect thermal conductivity, we utilized a variety of measurements to confirm the stability and homogeneity of CNTs in suspension and in tissue phantoms. Prior to measurement of the thermal conductivity of tissue phantoms containing CNTs, DLS and ELS were used to measure CNT stability in liquid suspension. DLS of CNT suspensions (CNT in a 1% Pluronic solution) shows that after 7 days, the size distribution remains unimodal and narrow (Fig. 6), indicating minimal precipitation within samples.

ELS measurements provide additional information about CNT colloid stability. ELS is a measurement of particle velocity at a known electric field strength, from which electrophoretic mobility can be calculated and related to zeta potential. Although this relationship is typically used under the assumption that particles are spherical in shape, many groups have still used this method when characterizing nanotubes, noting that it may overestimate the actual zeta potential.[47,53] Zeta potential is a useful parameter because it is a measure of the electric potential between the particle and its dispersion medium. Literature suggests various zeta potential limits that define colloid stability; however, frequently a zeta potential of at least ±15 mV is defined as a stable colloid suspension.[47,53] ELS of SWNT, MWNT, and SWNH suspensions resulted in zeta potential values of −24.2, −33.8, and −27.9 mV, respectively (Fig. 7). Therefore, each of the CNT suspensions prior to incorporation into sodium alginate could be considered stable. Sodium alginate should have no effect on CNT stability because it is neutral; however, this could not be confirmed with DLS or ELS because of the increased viscosity of these samples.

Therefore, to determine the CNT homogeneity throughout the tissue representative phantoms, TEM and Raman spectroscopy were employed. Cross-sectional TEM imaging of the CNT phantoms confirmed uniform distributions of CNTs throughout the specimen after cross-linking. Figure 8 below suggests homogeneous distribution of MWNTs throughout the phantom. Phantoms containing SWNHs and SWNTs yielded similar results (data not shown).

Raman spectroscopy was used to further confirm the DLS, ELS, and TEM results. Raman images were obtained by mapping the measured Raman intensity integrated over the selected spectral ranges of 1450–1700 cm^{-1}, which is also known as the carbonaceous nanoparticle G band, for each step in the scanned dimension. This band was selected to determine CNT–phantom homogeneity throughout the samples

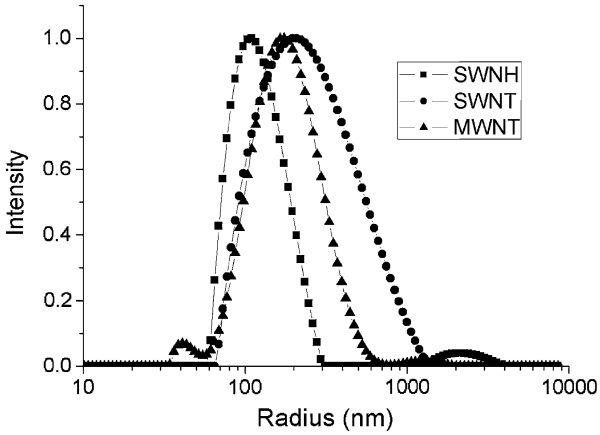

FIGURE 6. Dynamic light scattering of SWNTs, SWNHs, and MWNTs in 1% w/v Pluronic F-127 (0.05 mg/mL).

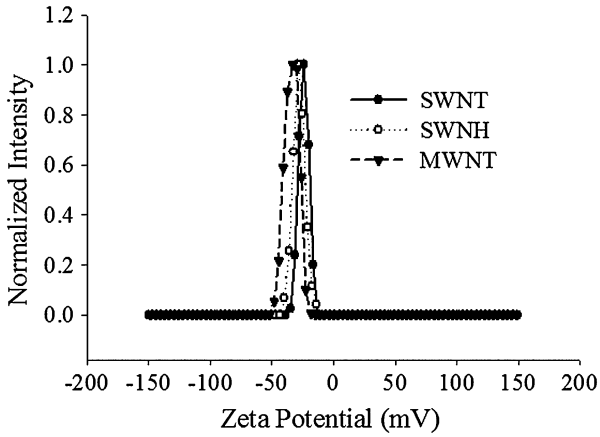

FIGURE 7. Zeta potential measurements of SWNTs, MWNTs, and SWNHs in 1% w/v Pluronic F-127 solution (0.1 mg/mL).

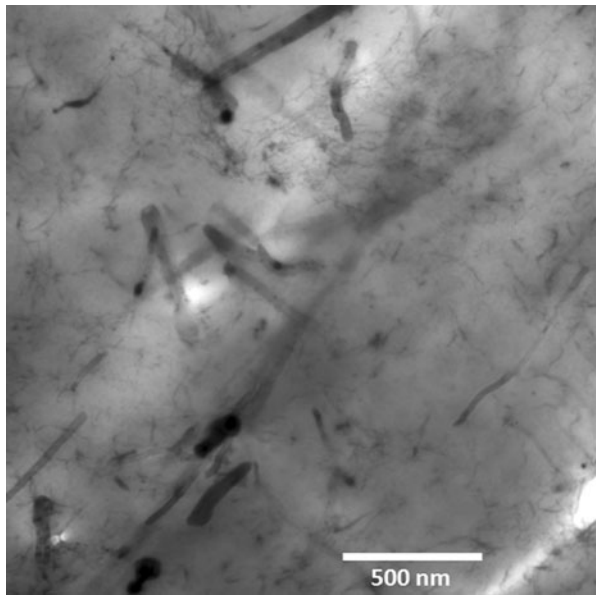

FIGURE 8. TEM image of MWNTs incorporated in phantom (0.1 mg/mL).

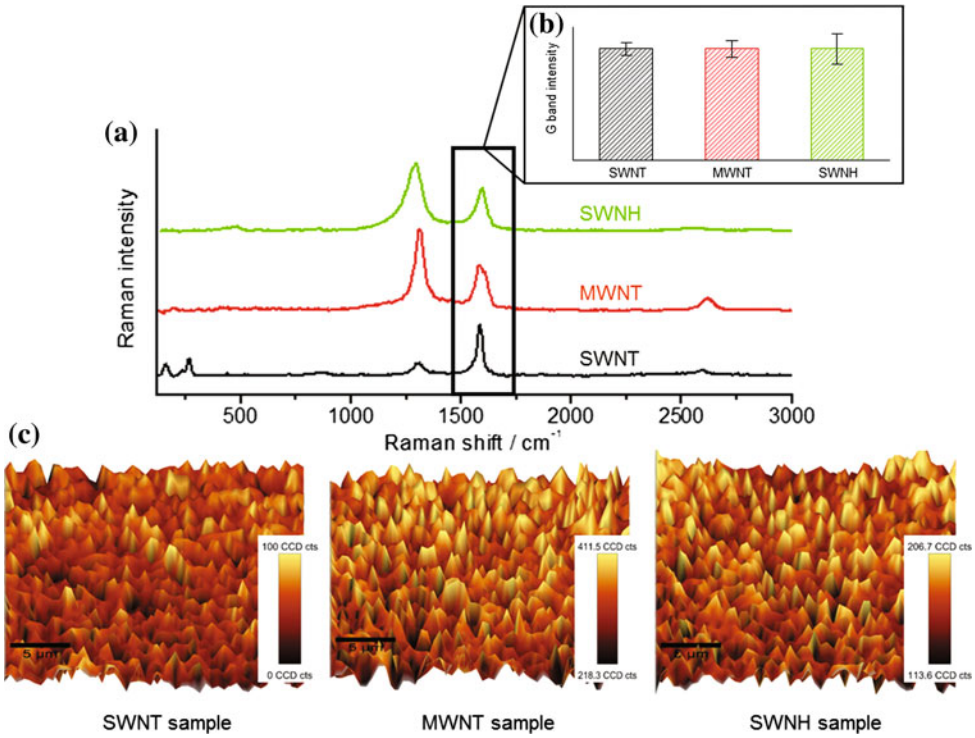

FIGURE 9. Raman spectroscopy of CNT phantoms. (a) Averaged Raman spectra of phantoms containing 1.0 mg/mL SWNT, MWNT, and SWNH, the black outline represents the integration region (G band). (b) Normalized Raman intensity of the G band ± the standard deviation over the four randomly scanned areas. (c) 3-D reconstruction of integrated regions for a 25 × 25 μm section of each sample. The color scale bars are indicated for each sample.

because it was the strongest peak common between the three CNT spectra. Figure 9a is the Raman spectra for each CNT–phantom sample averaged over four 25 × 25 μm sections. The relative standard deviations were calculated to be 5.8, 7.7, and 13.3% for phantoms containing SWNTs, MWNTs, and SWNHs, respectively. Their relative standard deviations (RSD) (Fig. 9b) and mapped G band intensities (Fig. 9c) suggest that the CNTs are homogeneously distributed in all cases. Results suggested minimal CNT precipitation throughout the phantoms. Variations in the average G band intensity for the four scanned areas are apparent because water was constantly evaporating from the phantom surface. Prior to each scan, the substrate was manually focused producing an additional source of error as the focal point varied throughout the measurements. Additionally, some areas produced a fluorescent signal, possibly due to laser-induced photo-damage of CNTs, which skewed the average intensity observed over the scanned area.

Thermal Conductivity of Phantoms with CNTs

Thorough characterization of the CNT phantoms suggested minimal precipitation; therefore, thermal conductivities of these samples could be measured. Thermal conductivities of phantoms containing SWNTs, MWNTs, and SWNHs of varying concentrations (0.1, 0.5, and 1.0 mg/mL) were determined in a similar manner as discussed for the agar gel and phantoms without CNTs. Six samples were used for each experimental group and the thermal conductivity was measured five times per group. The average slopes were determined for all samples using the range $\ln(t) = 1.35$–3 because it provided the highest R^2 values, 0.9785–0.9913, for each experimental group. Although, the slope and corresponding thermal conductivity of the samples varied slightly, since all slopes were determined at an identical location ($\ln(t) = 1.35$–3) and within the same data range, thermal conductivities can be compared. Thermal conductivities of all CNT–phantom composites are shown in Fig. 10. The error limits for the data in Fig. 10 were computed from the total estimated uncertainty (5.46%). In order to validate the total estimated uncertainty, the error estimate was compared with the standard deviation for all CNT phantoms. Standard deviations associated with the thermal conductivity of phantoms containing SWNTs, SWNHs, and MWNTs for a concentration of 1 mg/mL were determined to be ±0.015, ±0.018, and ±0.023 W/m·K, respectively. Standard deviations associated with the thermal conductivity of phantoms containing SWNTs, SWNHs, and MWNTs for a concentration of 1.0 mg/mL were determined to be

±0.015, ±0.018, and ±0.023 W/m·K, respectively, with corresponding standard deviations of ±0.019, ±0.02, and ±0.026 W/m·K, respectively.

The thermal conductivity of each type of CNT–phantom composite was observed to have a linear relationship with CNT concentration (0.1, 0.5, and 1.0 mg/mL). For instance, if the concentration of CNTs was increased by 10 times (0.1–1 mg/mL), the thermal conductivities of phantoms containing SWNTs, SWNHs, and MWNTs increased 10, 26, and 38, respectively (Fig. 10). Incorporating 0.1 mg/mL of SWNTs, SWNHs, and MWNTs into phantoms increased the thermal conductivity by 13, 4, and 20%, respectively, compared to pure sodium alginate. Thermal conductivities of phantoms increased by 24, 30, and 66% for phantoms containing 1.0 mg/mL SWNTs, SWNHs, and MWNTs, respectively, compared to pure sodium alginate. MWNT–phantom composites provided the highest thermal conductivity compared to other CNT phantoms. Thermal conductivities of phantoms containing SWNTs were superior to phantoms with SWNH inclusion in the concentration range of 0.1–0.5 mg/mL. However, inclusion of SWNHs increased thermal conductivity more significantly than SWNTs for concentrations higher than 0.5 mg/mL. Thermal conductivities for all CNT–phantom composites with estimated errors (determined from uncertainty analysis) are presented in Table 3.

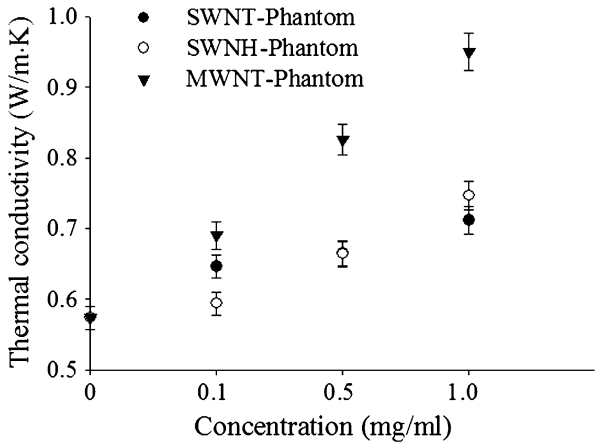

FIGURE 10. Thermal conductivities of CNT–phantom composites with varying CNT type and concentration.

DISCUSSION

This study elucidated the effect of incorporating varying CNT type (SWNT, MWNT, and SWNH) and concentration (0.1, 0.5, and 1.0 mg/mL) on the thermal conductivity of tissue representative phantoms. Sodium alginate was selected to represent tissue since its thermal conductivity (0.5737 W/m·K) is very close to that of human tissue (0.5–0.58 W/m·K).[4,13,15,33,43] Although the interfacial thermal conductance of CNTs in liquid suspension has been measured in other studies,[28,34] the thermal conductivity of CNTs in tissue or tissue representative phantoms has not been determined. The hot wire probe method was utilized due to its accuracy and ease of use for measuring the thermal conductivity of suspensions and solid samples.[4,33] The accuracy of our hot wire probe method was confirmed by comparing our measured thermal conductivity for glycerol and Styrofoam with previously reported values acquired by the dual-thermistor probe method[59] and pulse-decay method.[11] This coincides with prior studies using the hot wire probe, which measured thermal conductivities of agar gel, Styrofoam, gelatin, and cow liver and demonstrated an uncertainty of 4%.[4]

Effect of Concentration

CNT concentrations of 0.1, 0.5, and 1.0 mg/mL were selected because previous research has shown CNT concentrations lower than 1.0 mg/mL to have minimal toxicity.[9,48,49] Furthermore, SWNT, MWNT, and SWNH concentrations in the range of 0.1–1.0 mg/mL used in combination with laser heating have been shown to produce significant heat generation for effective photothermal based tumor destruction and regression in both *in vitro* and *in vivo* studies.[9,45,49] The greatest increase in thermal conductivity was observed for the highest CNT concentration (1.0 mg/mL). Increasing CNT concentration from 0.1 to 1.0 mg/mL caused the thermal conductivity of phantoms

TABLE 3. Thermal conductivities of CNT–phantom composites.

Concentration (mg/mL)	Thermal conductivity (W/m·K)			
	Phantom	Phantom–SWNT	Phantom–SWNH	Phantom–MWNT
0	0.5737 ± 0.016	–	–	–
0.1	–	0.6464 ± 0.017	0.5941 ± 0.016	0.6901 ± 0.019
0.5	–	0.6654 ± 0.018	0.6636 ± 0.018	0.8253 ± 0.022
1	–	0.71152 ± 0.019	0.7463 ± 0.02	0.9495 ± 0.026

containing SWNTs, SWNHs, and MWNTs to increase by 24, 30, and 66%, respectively. For concentrations of 1.0 mg/mL, thermal conductivities of phantoms containing MWNTs and SWNHs were 1.33 and 1.05 times higher, respectively, than phantoms containing SWNTs. Concentrations greater than 1.0 mg/mL may cause cells to experience reduced cell proliferation.[52] However, many epithelial based tumors (e.g., skin, bladder, prostate) are amenable to localized direct injection of CNTs into the tumor followed by laser treatment.[9] In this instance, optimum light absorption and thermal conductivity is desired; therefore, increasing CNT concentration above 0.1 mg/mL may be beneficial. Furthermore, by injecting CNTs directly into tumors or preferentially targeting tumor cells with CNTs conjugated to tumor specific antibodies or biomolecules (e.g., folic acid), we can supply a high concentration of CNTs in the desired tumor regions, thereby locally increasing optical absorption and thermal conductivity. By selectively depositing CNTs in the tumor region using methods described above, we can reduce associated toxicity due to high CNT concentration in healthy tissue.

Effect of Interfacial Thermal Resistance

SWNTs, SWNHs, and MWNTs possess exceptionally high thermal conductivities of 3000–6000 W/m·K; however, inclusion of CNTs in sodium alginate phantoms did not increase the thermal conductivity of the overall CNT–phantom composites substantially. This is potentially due to the high interfacial thermal resistance between CNTs and sodium alginate. These results are in close agreement with the effect of interfacial thermal resistance at the CNT–matrix interface described by Huxtable *et al.* and Merabia *et al.*[28,34] Measured thermal conductivities of CNT composites were determined to be less than thermal conductivities computationally calculated by Nan *et al.*[40,41] when interfacial thermal resistances were not considered. Thermal conductivity could be increased 5–20 times if interfacial thermal resistance was considered negligible.

Diameter Effects of CNTs in Tissue Composites

MWNT–phantom composites provided the highest thermal conductivity compared to other CNT composites. This is most likely due to their larger diameter (40–60 nm). Despite this advantage, the intrinsic thermal conductivity of MWNTs (3000 W/m·K) is lower than that of SWNTs (6000 W/m·K). Our experimental results exhibit close agreement with the computational results of Nan *et al.,* who demonstrated with an effective medium approach that MWNT-composites should have higher thermal conductivity than SWNT-composites due to the larger diameter of MWNTs.[41] Due to the smaller diameter of SWNTs (less than 2 nm), thermal conductivities of SWNT–phantom composites increased gradually with higher CNT concentration. However, for SWNH–phantom composites, thermal conductivities exceeded those of SWNT–phantom composites for concentrations greater than 0.5 mg/mL. Individual SWNHs are held together by van der Waals forces, forming flower-like structures with overall diameters of 50–100 nm. This difference in structure has been shown[19,45,54,56] to influence optical properties, potentially affecting thermal conductivity. We hypothesize that SWNHs at high concentrations may have added photoabsorptive benefits compared to SWNTs.

CONCLUSION

This is the first study investigating the impact of CNT inclusion on the thermal conductivity of tissue representative phantoms containing varying type and concentration of CNTs. Inclusion of MWNTs in the tissue phantom caused the greatest increase in thermal conductivity compared to all CNTs. Thermal conductivities for all CNT–phantom composites were in close agreement with previously published computational model predictions. It is anticipated that inclusion of CNTs in normal and tumor tissue will exhibit similar trends to those observed for sodium alginate phantoms. The composite thermal conductivity of phantoms containing CNTs did not increase as significantly as expected, most likely due to the existence of interfacial thermal resistance. However, even slight increases in thermal conductivity can provide beneficial gains in thermal diffusion. Knowledge of the composite thermal conductivity permits comparison of the thermal diffusion properties of tissues containing various CNT types. The measured thermal conductivity values for CNT–phantom composites can provide more accurate input parameters necessary for development of computational models for predicting laser heating of CNTs in tissue.

ACKNOWLEDGMENTS

This research was funded by the following sources: National Institute of Health Grant 1 R21 CA135230-01, National Science Foundation Grants CBET 0731108 and Early CAREER Award CBET 0955072, and an Institute for Critical Technology and Applied Science Grant (ICTAS, Virginia Tech). We would also

like to thank Dr. David Geohegan from Oak Ridge National Laboratories for kindly providing the single-walled carbon nanohorns and Dr. David Carroll's group from Wake Forest University for further chemical modification of the multi-walled nanotubes to achieve appropriate lengths.

REFERENCES

[1]Anderson, R. R., and J. A. Parrish. The optics of human-skin. *J. Invest. Dermatol.* 77:13–19, 1981.
[2]Arkin, H., K. R. Holmes, M. M. Chen, and W. G. Bottje. Thermal pulse decay method for simultaneous measurement of local thermal conductivity and blood perfusion: a theoretical analysis. *J. Biomech. Eng.* 108:208–214, 1986.
[3]Bassil, A., P. Puech, L. Tubery, W. Bacsa, and E. Flahaut. Controlled laser heating of carbon nanotubes. *Appl. Phys. Lett.* 88:1731131–1731133, 2006.
[4]Bhattacharya, A., and R. L. Mahajan. Temperature dependence of thermal conductivity of biological tissues. *Physiol. Meas.* 24:769–783, 2003.
[5]Bhavaraju, N. C., H. Cao, D. Y. Yuan, J. W. Valvano, and J. G. Webster. Measurement of directional thermal properties of biomaterials. *IEEE Trans. Biomed. Eng.* 48:261–267, 2001.
[6]Blackwell, J. H. A transient-flow method for determination of thermal constants of insulating materials in bulk part I—theory. *J. Appl. Phys.* 25:137–144, 1954.
[7]Brown, E., L. Hao, J. C. Gallop, and J. C. Macfarlane. Ballistic thermal and electrical conductance measurements on individual multiwall carbon nanotubes. *Appl. Phys. Lett.* 87:0231071–0231073, 2005.
[8]Bryning, M. B., D. E. Milkie, M. F. Islam, J. M. Kikkawa, and A. G. Yodh. Thermal conductivity and interfacial resistance in single-wall carbon nanotube epoxy composites. *Appl. Phys. Lett.* 87:161909, 2005.
[9]Burke, A., X. F. Ding, R. Singh, *et al.* Long-term survival following a single treatment of kidney tumors with multi-walled carbon nanotubes and near-infrared radiation. *Proc. Natl. Acad. Sci. U.S.A.* 106:12897–12902, 2009.
[10]Carslaw, H. S., and J. C. Jaeger. Conduction of Heat in Solids (2nd ed.). Oxford: Clarendon Press, 1959.
[11]Chen, M. M., K. R. Holmes, and V. Rupinskas. Pulse-decay method for measuring the thermal-conductivity of living tissues. *J. Biomech. Eng. Trans. ASME* 103:253–260, 1981.
[12]Clancy, T. C., and T. S. Gates. Modeling of interfacial modification effects on thermal conductivity of carbon nanotube composites. *Polymer* 47:5990–5996, 2006.
[13]Cohen, M. L. Measurement of the thermal properties of human skin. A review. *J. Investig. Dermatol.* 69:333–338, 1977.
[14]Dresselhaus, M. S., G. Dresselhaus, and P. C. Eklund. Science of Fullerenes and Carbon Nanotubes. San Diego: Academic Press, 1996.
[15]Ducharme, M. B., and P. Tikuisis. In vivo thermal conductivity of the human forearm tissues. *J. Appl. Physiol.* 70:2682–2690, 1991.
[16]Eletskii, A. V. Transport properties of carbon nanotubes. *Phys. Usp.* 52:209–224, 2009.
[17]Fan, X., *et al.* Isolation of carbon nanohorn assemblies and their potential for intracellular delivery. *Nanotechnology* 18:195103, 2007.
[18]Figliola, R. S., and D. E. Beasley. Theory and Design for Mechanical Measurements (2nd ed.). Hoboken, NJ: John Wiley, 1995.
[19]Fisher, J. W., S. Sarkar, C. F. Buchanan, C. S. Szot, J. Whitney, H. C. Hatcher, S. V. Torti, C. G. Rylander, and M. N. Rylander. Photothermal response of human and murine cancer cells to multiwalled carbon nanotubes after laser irradiation. *Cancer Res.* 70:9855–9864, 2010.
[20]Fujii, M., X. Zhang, H. Xie, *et al.* Measuring the thermal conductivity of a single carbon nanotube. *Phys. Rev. Lett.* 95:065502, 2005.
[21]Gao, L., X. Zhou, and Y. Ding. Effective thermal and electrical conductivity of carbon nanotube composites. *Chem. Phys. Lett.* 434:297–300, 2007.
[22]Gummow, R. J., and I. Sigalas. Generalised hot-wire technique for high pressure thermal conductivity measurements. *J. Phys. E* 21:442, 1988.
[23]Gun'kin, I., and N. Loginova. Effect of nature of organic solvent on the absorption spectrum of C60 fullerene. *Russ. J. Gen. Chem.* 76:1911–1913, 2006.
[24]Hill, J. E., J. D. Leitman, and J. E. Sunderland. Thermal conductivity of various meats. *Food Technol.* 21:1143–1148, 1967.
[25]Hirsch, L. R., R. J. Stafford, J. A. Bankson, *et al.* Nanoshell-mediated near-infrared thermal therapy of tumors under magnetic resonance guidance. *Proc. Natl. Acad. Sci. U.S.A.* 100:13549–13554, 2003.
[26]Holmes, K. R., and M. M. Chen. Local thermal conductivity of Para-7 fibrosarcoma in hamster. In: 1979 Advances in Bioengineering. New York: ASME, 1979, pp. 147–149.
[27]Hone, J., M. Whitney, and A. Zettl. Thermal conductivity of single-walled carbon nanotubes. *Synth. Met.* 103:2498–2499, 1999.
[28]Huxtable, S. T., D. G. Cahill, S. Shenogin, *et al.* Interfacial heat flow in carbon nanotube suspensions. *Nat. Mater.* 2:731–734, 2003.
[29]Iijima, S., M. Yudasaka, R. Yamada, *et al.* Nano-aggregates of single-walled graphitic carbon nano-horns. *Chem. Phys. Lett.* 309:165–170, 1999.
[30]Kam, N. W. S., M. O'Connell, J. A. Wisdom, and H. J. Dai. Carbon nanotubes as multifunctional biological transporters and near-infrared agents for selective cancer cell destruction. *Proc. Natl. Acad. Sci. U.S.A.* 102:11600–11605, 2005.
[31]Lee, C. S. D., J. P. Gleghorn, N. Won Choi, M. Cabodi, A. D. Stroock, and L. J. Bonassar. Integration of layered chondrocyte-seeded alginate hydrogel scaffolds. *Biomaterials* 28:2987–2993, 2007.
[32]Levi-Polyachenko, N. H., D. L. Carroll, and J. H. Stewart. Applications of carbon-based nanomaterials for drug delivery in oncology. In: Medicinal Chemistry and Pharmacological Potential of Fullerences and Carbon Nanotubes, edited by F. Cataldo and T. Ros. Netherlands: Springer, 2008, pp. 223–266.
[33]Liang, X. G., X. S. Ge, Y. P. Zhang, and G. J. Wang. A convenient method of measuring the thermal-conductivity of biological tissue. *Phys. Med. Biol.* 36:1599–1605, 1991.
[34]Merabia, S., S. Shenogin, L. Joly, P. Keblinski, and J.-L. Barrat. Heat transfer from nanoparticles: a corresponding state analysis. *Proc. Natl. Acad. Sci.* 106:15113–15118, 2009.

[35]Miyako, E., H. Nagata, K. Hirano, K. Sakamoto, Y. Makita, K. Nakayama, and T. Hirotsu. Photoinduced antiviral carbon nanohorns. *Nanotechnology* 19:4751031–4751037, 2008.
[36]Miyako, E., H. Nagata, K. Hirano, M. Makita, K. Nakayama, T. Hirotsu, *et al*. Near-infrared laser-triggered carbon nanohorns for selective elimination of microbes. *Nanotechnology* 18:4751031–4751037, 2007.
[37]Miyawaki, J., M. Yudasaka, T. Azami, Y. Kubo, and S. Iijima. Toxicity of single-walled carbon nanohorns. *ACS Nano* 2:213–226, 2008.
[38]Moffat, R. J. Describing the uncertainties in experimental results. *Exp. Therm. Fluid Sci.* 1:3–17, 1988.
[39]Monteiro-Riviere, N. A., R. J. Nemanich, A. O. Inman, Y. Y. Y. Wang, and J. E. Riviere. Multi-walled carbon nanotube interactions with human epidermal keratinocytes. *Toxicol. Lett.* 155:377–384, 2005.
[40]Nan, C.-W., R. Birringer, D. R. Clarke, and H. Gleiter. Effective thermal conductivity of particulate composites with interfacial thermal resistance. *J. Appl. Phys.* 81:6692–6699, 1997.
[41]Nan, C. W., G. Liu, Y. H. Lin, and M. Li. Interface effect on thermal conductivity of carbon nanotube composites. *Appl. Phys. Lett.* 85:3549–3551, 2004.
[42]Nix, G. H., G. W. Lowery, R. I. Vachon, and G. E. Tanger. Direct determination of thermal diffusivity and conductivity with a refined line-source technique. *Process Aeronaut. Astronaut.: Thermophys. Spacecraft Planet. Bodies* 20:865–878, 1967.
[43]Poppendiek, H. F., R. Randall, J. A. Breeden, J. E. Chambers, and J. R. Murphy. Thermal conductivity measurements and predictions for biological fluids and tissues. *Cryobiology* 3:318–327, 1966.
[44]Rafii-Tabar, H. Computational Physics of Carbon Nanotubes. Cambridge, UK: Cambridge University Press, 2008.
[45]Sarkar, S., J. Fisher, C. Rylander, and M. N. Rylander. Photothermal response of tissue phantoms containing multi-walled carbon nanotubes. *J. Biomech. Eng.* 132:044505, 2010.
[46]Scheffy, W. J., and E. F. Johnson. Thermal conductivities of liquids at high temperatures. *J. Chem. Eng. Data* 6:245–249, 1961.
[47]Sun, Z., V. Nicolosi, D. Rickard, S. D. Bergin, D. Aherne, and J. N. Coleman. Quantitative evaluation of surfactant-stabilized single-walled carbon nanotubes: dispersion quality and its correlation with zeta potential. *J. Phys. Chem. C* 112:10692–10699, 2008.
[48]Sun, X., R. Q. Yu, G. Q. Xu, T. S. A. Hor, and W. Ji. Broadband optical limiting with multiwalled carbon nanotubes. *Appl. Phys. Lett.* 73:3632–3634, 1998.
[49]Torti, S. V., F. Byrne, O. Whelan, *et al*. Thermal ablation therapeutics based on CNx multi-walled nanotubes. *Int. J. Nanomed.* 2:707–714, 2007.
[50]Touloukian, Y. S., P. E. Liley, and S. C. Saxena. Thermophysical Properties of Matter. New York: Plenum Publishing Corporation, 1970.
[51]Valvano, J. W., J. R. Cochran, and K. R. Diller. Thermal-conductivity and diffusivity of biomaterials measured with self-heated thermistors. *Int. J. Thermophys.* 6:301–311, 1985.
[52]Warheit, D. B., B. R. Laurence, K. L. Reed, D. H. Roach, G. A. M. Reynolds, and T. R. Webb. Comparative pulmonary toxicity assessment of single-wall carbon nanotubes in rats. *Toxicol. Sci.* 77:117–125, 2004.
[53]White, B., S. Banerjee, S. O'Brien, N. J. Turro, and I. P. Herman. Zeta-potential measurements of surfactant-wrapped individual single-walled carbon nanotubes. *J. Phys. Chem. C* 111:13684–13690, 2007.
[54]Whitney, J. R., S. Sarkar, J. Zhang, *et al*. Single walled carbon nanohorns as photothermal cancer agents. *Lasers Surg. Med.* 43:43–51, 2011.
[55]Wong, M. Alginates in tissue engineering. In: Biopolymer Methods in Tissue Engineering, edited by Springerlink. New Jersey: Humana Press, Inc., 2003, pp. 77–86.
[56]Yehia, H. N., R. K. Draper, C. Mikoryak, *et al*. Single-walled carbon nanotube interactions with HeLa cells. *J. Nanobiotechnol.* 5:8, 2007.
[57]Yi, W., L. Lu, Z. Dian-lin, Z. W. Pan, and S. S. Xie. Linear specific heat of carbon nanotubes. *Phys. Rev. B* 59:R9015, 1999.
[58]Yi, M., H. V. Panchawagh, R. J. Podhajsky, and R. L. Mahajan. Micromachined hot-wire thermal conductivity probe for biomedical applications. *IEEE Trans. Biomed. Eng.* 56:2477–2484, 2009.
[59]Zhang, H. F., L. Q. He, S. X. Cheng, Z. T. Zhai, and D. Y. Gao. A dual-thermistor probe for absolute measurement of thermal diffusivity and thermal conductivity by the heat pulse method. *Meas. Sci. Technol.* 14:1396–1401, 2003.
[60]Zhang, M., T. Murakami, K. Ajima, *et al*. Fabrication of ZnPc/protein nanohorns for double photodynamic and hyperthermic cancer phototherapy. *Proc. Natl. Acad. Sci. U.S.A.* 105:14773–14778, 2008.